




Impedance response behavior and mechanism study of axon-like ionic conductive cellulose-based hydrogel strain sensor

Dianbo Zhang^{1,2,3} · Minyue Zhang^{1,2} · Jingwen Wang^{1,2} · Hongling Sun^{1,2} · Hu Liu^{1,2}  · Liwei Mi³ · Chuntai Liu^{1,2} · Changyu Shen^{1,2}

Received: 18 January 2022 / Revised: 11 February 2022 / Accepted: 18 February 2022 / Published online: 13 April 2022
© The Author(s), under exclusive licence to Springer Nature Switzerland AG 2022

Abstract

As a promising candidate for flexible epidermal strain sensor, the obvious resistance sensing signal drift of ionic conductive hydrogel affects its practical application significantly, and the AC impedance analysis appears to be an effective test method. Here, the rarely reported impedance sensing mechanism was investigated based on an axon-like ionic conductive hydrogel strain sensor, which is composed of cellulose hydrogel particles (CHPs) as the core sensing medium, rubber tube as the elastic cortex, and stainless steel as the electrode. Specifically, the prepared hydrogel strain sensor exhibited a negative ion concentration-dependent impedance sensing behavior, the impedance variation ($\Delta Z/Z_0$) and sensitivity (GF) at 400% reach 441.5 and 630.1, respectively. What is more, the AC impedance sensing behavior of the hydrogel sensor displayed good strain amplitude identifiability in a wide strain range up to 400%, ultralow detection limit (0.1% strain), excellent rate independence, and outstanding long-term fatigue resistance. Importantly, an equivalent circuit model was built, and the variation of ion transport impedance and electric double-layer capacitance at the electrode-CHPs interface during the tension process were verified to be the internal sensing mechanism. What is more, the special skin-core structure can effectively solve the dehydration problem and poor mechanical property of hydrogel, and the amounts of interfaces between adjacent CHPs are also beneficial for improving the impedance responsivity. We believe the proposed impedance response mechanism will undoubtedly provide important guidance for the design of high-performance ionic conductive hydrogel strain sensor.

Keywords Ionic conductive hydrogel · Strain sensor · AC impedance · Response mechanism · Equivalent circuit

1 Introduction

With the development of artificial intelligence, high-performance wearable strain sensors are highly demanded in the fields of physiological signal monitoring [1–3], motion detection [4–6], human–machine interfaces [7–10],

intelligent robotics [11–13], and so on. Owing to the brilliant characteristics of self-healing, high stretchability, surface compliance, and good biocompatibility, ionic conductive hydrogels have aroused great attentions to be used as the promising materials for next-generation flexible epidermal strain sensors [14–17].

Due to the unique structure of three-dimensional cross-linked polymer networks and the amount of adsorbed aqueous solution, there are still some enormous challenges to be solved. For instance, the dehydration of hydrogels is easy to cause the attenuation of sensing capacity, elastic deterioration, and even complete failure of their strain sensor during the long-term outdoor use. Besides, the poor mechanical property of most hydrogels will undoubtedly restrict their application in most practical applications, so some enhancement methods are necessary, increasing the complexity and production cost. More importantly, the resistance sensing signal of most ionic conductive hydrogel often exhibits obvious baseline drift and even inconsistent sensing signal with

✉ Hu Liu
liuhu@zzu.edu.cn

✉ Chuntai Liu
ctliu@zzu.edu.cn

¹ Key Laboratory of Materials Processing and Mold, Ministry of Education, Zhengzhou University, Zhengzhou 450002, Henan, China

² National Engineering Research Center for Advanced Polymer Processing Technology, Zhengzhou University, Zhengzhou 450002, Henan, China

³ Center for Advanced Materials Research, Zhongyuan University of Technology, Zhengzhou 450007, Henan, China

strain, which can be attributed to the accumulation of ions at the interface between hydrogel and electrode under a DC filed, forming an electrical double-layer capacitance (EDLC) and incomplete loop in the circuit.

Recently, enormous efforts have been conducted to solve the problems stated above. For instance, the application of non-volatile solvent [18–21] and high salt concentration [22–25] can effectively overcome the dehydration problem of hydrogels and greatly expand the service temperature of their sensor, but the high sensitivity of those response medium to environmental humidity is still inevitable. What is more, the addition of electronic conductive network [26–28] and rational structure design of hydrogel strain sensors [29, 30] can also effectively improve their responsiveness, but the complex and costly processing process is still necessary. Furthermore, AC impedance method has been applied to investigate the strain sensing behavior of ionic conductive hydrogel strain sensor [17, 31–34]. Under the excitation of AC signal, the conductive ions in the hydrogel were cyclic reciprocating motion, forming a complete loop with the external electronic circuit through the interfacial coupling of the EDLC, so that the baseline drift problem in the DC method can be effectively voided and stable sensing pattern was successfully achieved. However, the detail sensing mechanism of ionic conductive hydrogel strain sensor working in the AC test mode is still not deeply analyzed.

Inspired by the fidelity transmission of nerve signals in axon, an environmental tolerant and highly sensitive axon-like ionic conductive hydrogel is constructed for flexible epidermal strain sensor. Similar to the axon, the skin–core structured strain sensor composed of cellulose hydrogel particles (CHPs) as the core sensing medium, rubber tube as the elastic cortex, and stainless steel as the electrode. Specifically, the effect of ion concentration on impedance sensing behavior upon tension was systematically studied, and an equivalent circuit model was built to analyze the detail sensing mechanism. Then, the strain amplitude and rate dependent impedance sensing performances and long-term stability of the hydrogel strain sensor were further studied. As a verification, combined with TENG which is a typical advanced wearable power source, the axon-like CHPs strain sensor shown a good performance in human motion and physiology signal detection. This study will provide great guidance for the widespread application of ionic conductive hydrogel in wearable strain sensor.

2 Experimental section

2.1 Materials and chemicals

α -Cellulose with a molecular weight of 162.06 was purchased from Aladdin (Shanghai, China). Epichlorohydrin

(ECH) was supplied by Tianjin Damao Chemical Reagent Factory (China). Sodium hydroxide (NaOH), urea, and sodium chloride (NaCl) were bought from Sinopharm Chemical Reagent Co. Ltd, China. All the materials and chemicals were used as received without treatment.

2.2 Preparation of cellulose hydrogel particle

Typically, 12 g cellulose powder was dispersed into 300 g aqueous solution containing 7 wt % NaOH and 12 wt % urea, which was then precooled in a $-18\text{ }^{\circ}\text{C}$ refrigerator for 12 h and mechanically stirred for 30 min to dissolve the cellulose completely. After that, transparent cellulose hydrogel was obtained by adding 30 mL ECH under vigorous stirring, cross-linking at $50\text{ }^{\circ}\text{C}$ for 8 h, and aging at room temperature for 48 h. After being soaked in deionized (DI) water to remove the remnant NaOH and urea until the PH value reaches 7, the resultant cellulose hydrogel with poor mechanical strength (Fig. S1) was smashed into particles using a blender and treated using a 20-mesh sieve followed by an 80-mesh sieve to remove the large and small particles. The final cellulose hydrogel particles (CHPs) were re-dispersed in DI water containing different NaCl concentrations (0.05 M, 0.154 M, 0.5 M, and 1 M) for 24 h to achieve a balance of ion changing, obtaining series of CHPs with different NaCl loading, which were named as CHPs-0.05, CHPs-0.15, CHPs-0.5, and CHPs-1, respectively.

2.3 Fabrication of CHPs-based strain sensor

For the preparation of CHPs-based strain sensor, CHPs were first squeezed into a rubber tube with an internal diameter of 1.6 mm, and two stainless steel electrodes were inserted into both ends to build a CHPs filled length of 12 mm. After that, the inserted stainless-steel electrodes were strongly tied, and an effective elastic length of 28 mm was created for the strain sensor.

2.4 Characterizations

Electrochemical impedance spectroscopy (EIS) and AC impedance as a function of time for strain sensor were measured using an electrochemical workstation (Chenhua CHI660E, China). In the frequency range of 0.1 Hz to 1 MHz, the AC potential and bias voltage was set to be 100 mV and 0 V for EIS test. The strain sensing performance of the sensor was studied through in-situ recording the AC impedance change using the electrochemical workstation coupled with a universal tensile testing machine (Suns UTM2203, China). Here, the applied AC potential, bias voltage, and testing frequency were set to be 100 mV, 0 V, and 1000 Hz, respectively.

3 Results and discussions

Inspired by the fidelity transmission of nerve signals in axon, as shown in Fig. 1a, an environmental tolerant and highly sensitive axon-like ionic conductive hydrogel strain sensor with a skin–core structure was designed. Figure 1b illustrates the preparation process of CHPs-based strain sensor, and the details are listed in the experiment part. The designed strain sensor consists of highly elastic cortex (rubber tube), core sensing medium (ionic conductive CHPs), and stainless-steel electrode. Specifically, rubber tube provides excellent stretch-recovery properties and good dehydration prevention of hydrogel, CHPs supplies conductive path and responds to the device deformation, and stainless-steel electrode is closely connected with the filled CHPs to form the interface of electronic circuit and ionic conductor. Figure 1c shows the optical picture of the filled CHPs which were squeezed onto a glass plate directly, of which a large number of irregular particles aggregate together closely to construct tight interfaces

without obvious void based on the existence of hydrogen bonding. Optical pictures of the CHPs-based strain sensor under releasing and stretching state are shown in Fig. 1d, e, and the red backlight can homogeneously transmit the rubber tube even when the strain sensor is stretched to 250% strain, indicating that the filled CHPs keeps densely aggregation without obvious fracture, which is conductive to endow the strain sensor with large sensing range.

For the practical application, excellent stretching-releasing performance is an essential characteristic that profoundly affects the stability and long-term durability of strain sensor. As shown in Figs. 2a and S2, the maximum stress keeps almost constant with a slight decrease of 4.5% over 500 cycles, and the energy loss coefficient displays an obvious decrease in the initial several cycles and then tends to be stable at 6.5% in the subsequent cycles. Meanwhile, it also exhibits a stable plastic deformation of 1.96% after a slight increase process. All these can be ascribed to the highly elastic rubber that lays the foundation for stable response characteristics of the CHPs-based strain sensor. Furthermore,

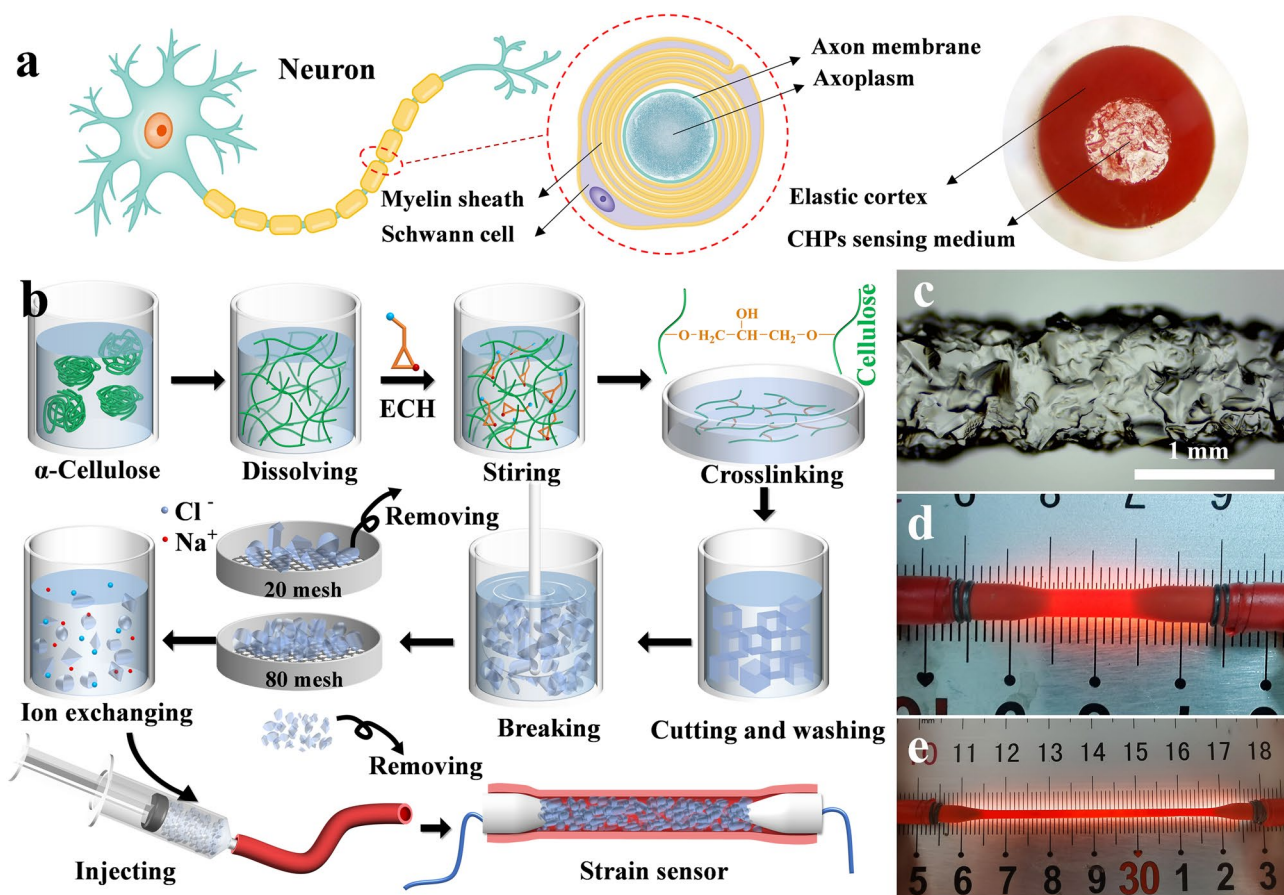


Fig. 1 a Schematic illustration showing the axon-like CHPs-based strain sensors and b its detail preparation process. c Optical picture of the filled gel particles in CHPs-based strain sensor. Optical pictures

of CHPs-based strain sensor under d releasing and e stretching state (250% strain)

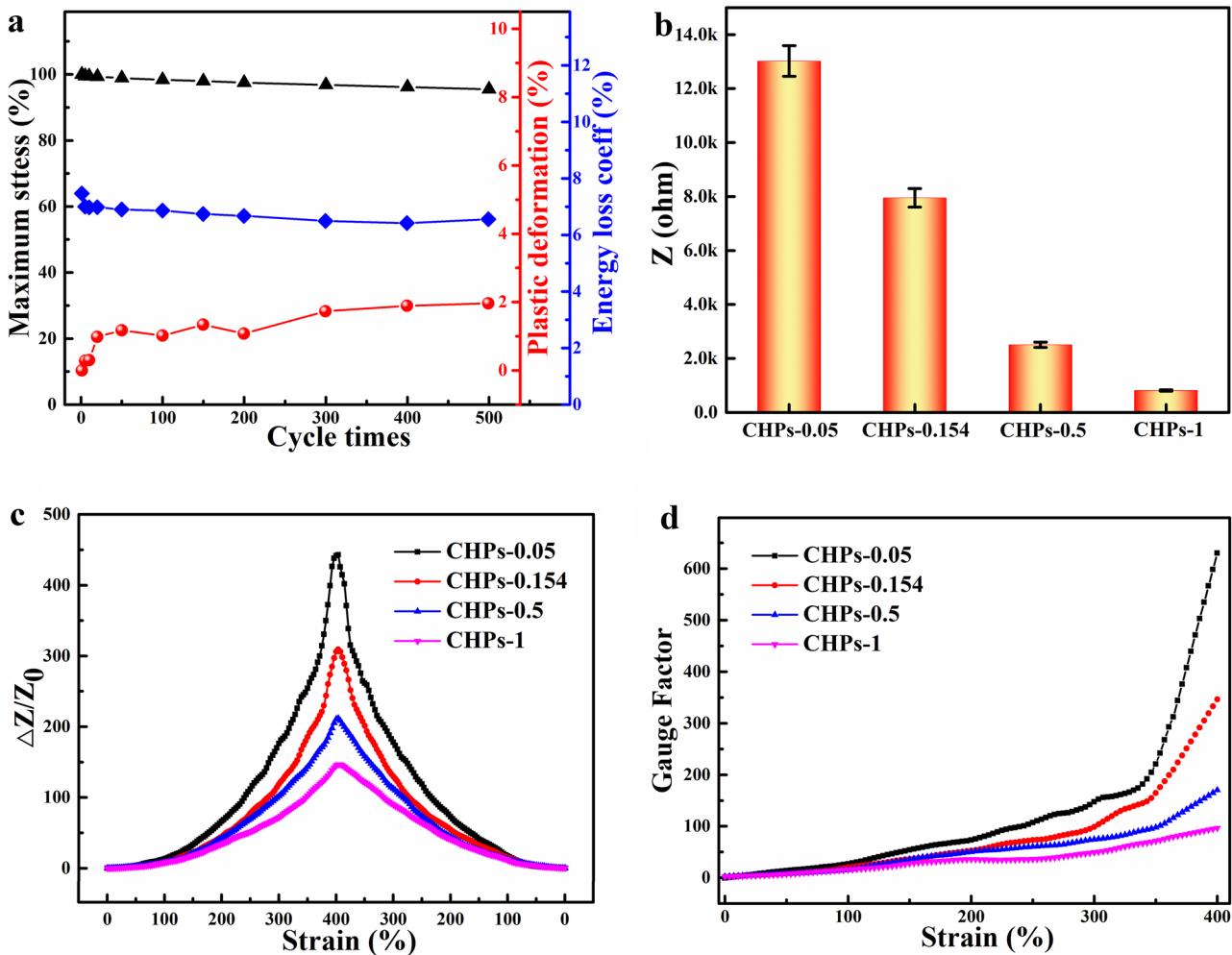


Fig. 2 **a** Cyclic tensile mechanical properties of CHPs-based strain sensor. **b** Impedance values of CHPs-based strain sensors with different ion concentrations. **c** Impedance response of CHPs-based strain sensors

the impedance value of the CHPs-based strain sensor with increasing ionic concentrations was tested to be 13,340 Ω, 8045 Ω, 2614 Ω, and 836 Ω for CHPs-0.05, CHPs-0.15, CHPs-0.5, and CHPs-1, respectively (Fig. 2b). Such an ionic concentration-dependent electrical property is mainly ascribed to the construction of perfect ionic conductive pathway under a higher ionic concentration. The influence of ionic concentration on the impedance response performance of the CHPs strain sensor was explored, and the relative impedance variation $\Delta Z/Z_0$ ($\Delta Z = Z - Z_0$, where Z is the impedance in the stretching state and Z_0 is the initial impedance) as a function of strain was depicted in Fig. 2c. Clearly, $\Delta Z/Z_0$ increases gradually during the stretching process up to 400% strain and then decreases gradually to the initial value during the releasing process for all CHPs-based strain sensors, and the obtained $\Delta Z/Z_0$ -strain curves display good symmetry in one stretching-releasing cycle, demonstrating excellent resilience and recoverability, which is unlike the baseline drift of the DC resistance sensing behavior of the

with different ion concentrations during one stretching-releasing process. **d** GF as a function of strain for CHPs-based sensor with different ion concentrations

reported ionic hydrogel strain sensor. What is more, CHPs with a higher ionic concentration produces a smaller $\Delta Z/Z_0$ under the same strain, indicating a lower sensitivity. Here, gauge factor (GF, the derivative of $\Delta Z/Z_0$ to the applied strain (ϵ)) is applied to evaluate the sensitivity of different strain sensors. As shown in Fig. 2d, all GFs show a linear increasing trend followed by a sharp increase after 350% strain. Specifically, the GF at 400% strain is calculated to be 630.1, 346.2, 171.1, and 96.5 for CHPs-0.05, CHPs-0.15, CHPs-0.5, and CHPs-1, respectively.

To explain the strain sensing mechanism, the circuit structure and equivalent circuit of the CHPs-based strain sensor are analyzed and shown in Fig. 3a. Specifically, the circuit of the sensor mainly contains the ion transport impedance in filled CHPs (R), the charge-transfer resistance across the electrode-CHPs interfaces (R_{ct}), the electric double-layer capacitance at the electrode-CHPs interface (CPE_{edl}), the induction capacitance between the two electrodes (CPE_{ic}), and the diffusion resistance of ion/electron in the electrode surface oxide layer

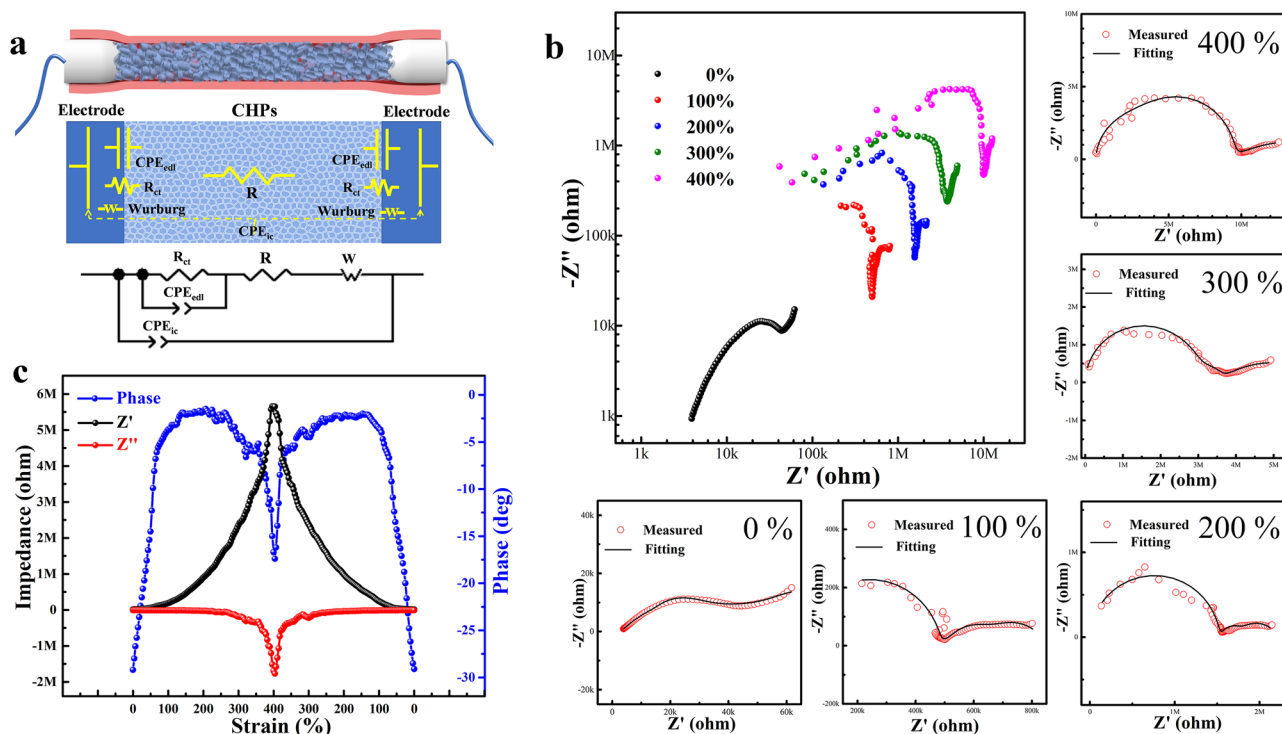


Fig. 3 **a** Schematic diagram showing the structure change of CHPs-based strain sensor and the corresponding equivalent circuit model. **b** The Nyquist-plots of the CHPs-0.05-based strain sensor under different strain amplitudes, the midpoint diagram of the small figure is the

measured data, and the solid line is the fitting result of the model circuit. **c** The variation of the real impedance (Z'), imaginary impedance (Z'') and phase of the CHPs-0.05-based strain sensor during a 400% stretching-releasing cycle

(Wurzburg, W). After being stretched, as shown in the Nyquist-plots of CHPs-0.05 under different strains (Fig. 3b), both the real and imaginary parts of impedance increase rapidly with increasing strain. Clearly, capacitance–resistance arcs in the high-frequency region and the diffusion slashes in the low-frequency region are observed for all Nyquist diagrams. In addition, the fitted curve of impedance spectra using the equivalent circuit are all in good coincidence with the test results, indicating that the established circuit model was consistent with the real situation of the device.

According to the simulated circuit parameters of the CHPs-0.05-based strain sensor shown in Table S1, it can be seen clearly that R increase from 5.12 $K\Omega$ at 0% strain to 5.92 $M\Omega$ at 400% strain, showing a much higher variation (1155 at 400%) than the theoretical result (105.8 at 400%) based on the resistivity model (Fig. S3). Hence, it can be concluded that the introduction of hydrogel particles which supplies amounts of interface between them plays an important impact on the ion transport behavior in filed CHPs, improving the strain impedance response of hydrogel-based devices significantly. Besides, the increasing strain also leads to the reduction of CPE_{edl} and the increase of R_{ct} and W due to the reduction of hydrogel-electrode contact area caused by the necking of the rubber tube, while CPE_{ic}

reduces based on the increased electrode spacing. Generally, the reduction of CPE_{edl} and CPE_{ic} implies an increased impedance.

Furthermore, the variation of the real impedance (Z'), imaginary impedance (Z''), and phase angle of CHPs-0.05-based strain sensor in a 400% stretching-releasing cycle are analyzed to support the above analysis. As depicted in Fig. 3c, Z' represents the charge carrier transport impedance and Z'' represents the capacitive impedance increase simultaneously with the increasing strain. In the low strain region, the growth rate of Z' is significantly faster than that of Z'' because of the good strain impedance response behavior of the filed CHPs and the necking of rubber tub is not obvious in this region, resulting in a gradual decreasing phase angle. In the high strain region, the necking of rubber tub becomes serious, the contribution of CPE_{edl} and R_{ct} , which describe the charge transfer behavior at the CHPs-electrode interfaces, to the total impedance increases significantly. As a result, Z'' displays a faster growth trend than that of Z' , and the phase angle becomes to be an increasing trend. Especially at the high strain range greater than 350%, the rapid increase of the Z'' significantly improves the response of the total impedance to strain, which is consistent with the mutation point of the linear growth of GF.

To evaluate the applicability of the prepared CHPs-based strain sensor, dynamic impedance response and sensing stability were systematically studied. As shown in Fig. 4a–c, the impedance response of CHPs-0.05-based strain sensor exhibits good discrimination and reproducibility for a wide strain ranging from 0.1 to 400%, and an ultralow limit of detection (LOD) of 0.1% was achieved, enabling it to monitor subtle and large deformation effectively. In addition, the response curves of the sensor keep excellent consistency under different strain rates (Fig. 4d), such a good rate-independent sensing behavior can ensure a precise and reliable detection when doing exercise. Furthermore, as depicted in Fig. 4e, the prepared sensor exhibits stable sensing pattern without obvious signal drift upon 50% tensile strain at a rate of 2 mm/s in a period of 10,000 s, demonstrating good long-term durability of the CHPs-based strain sensor. More importantly, the rubber tube can also effectively avoid the impedance response drift or failure caused by the dehydration of conventional hydrogel strain sensor, and the good durability of our prepared CHPs-based sensor can also be well maintained after being stored at room temperature for 6 months (Fig. 4f). All these undoubtedly make our prepared sensor to be workable in various application scenarios.

Owing to the abovementioned excellent AC impedance sensing performances, the axon-like CHPs-based strain sensor can be coupled with the advanced wearable power generator such as triboelectric nanogenerator (TENG)

and piezoelectric nanogenerator (PENG), which can provide weak alternating excitation signals. As shown in Figs. S4 and S5, a simple and efficient detection circuit composed of TENG, CHPs-based strain sensor, regulated diodes and ammeters is constructed, where the alternating current flowing through the sensor is inversely proportional to the recorded impedance sensing signal. As shown in Fig. 5a–d, CHPs-based strain sensor driven by TENG is employed to detect the elbow joint bending at 0°, 45°, 90°, and 135°, respectively. The strain sensor is stretched when the elbow joint of volunteer is bent, resulting in an increased impedance, and the alternating current through the device decreases obviously. The peak current response peak decreases monotonously as the bending angle increases, indicating that bending of elbow joint can be accurately tracked. Meanwhile, the response pattern also displays excellent stability and repeatability in the continuous interactive transformation of different elbow bending states (Fig. 5e–i and Video S1). As revealed in Fig. 5j, the wearable CHPs-based strain sensor is fixed on the volunteer's chest to detect human breathing, which is a significant physiological signal. It can be seen in Fig. 5k and Video S2 that shallow breathing and deep breathing are clearly discriminated from their different sensing patterns, implying the great potential application of the CHPs-based strain sensor to be applied for the real-time monitoring of apnea.

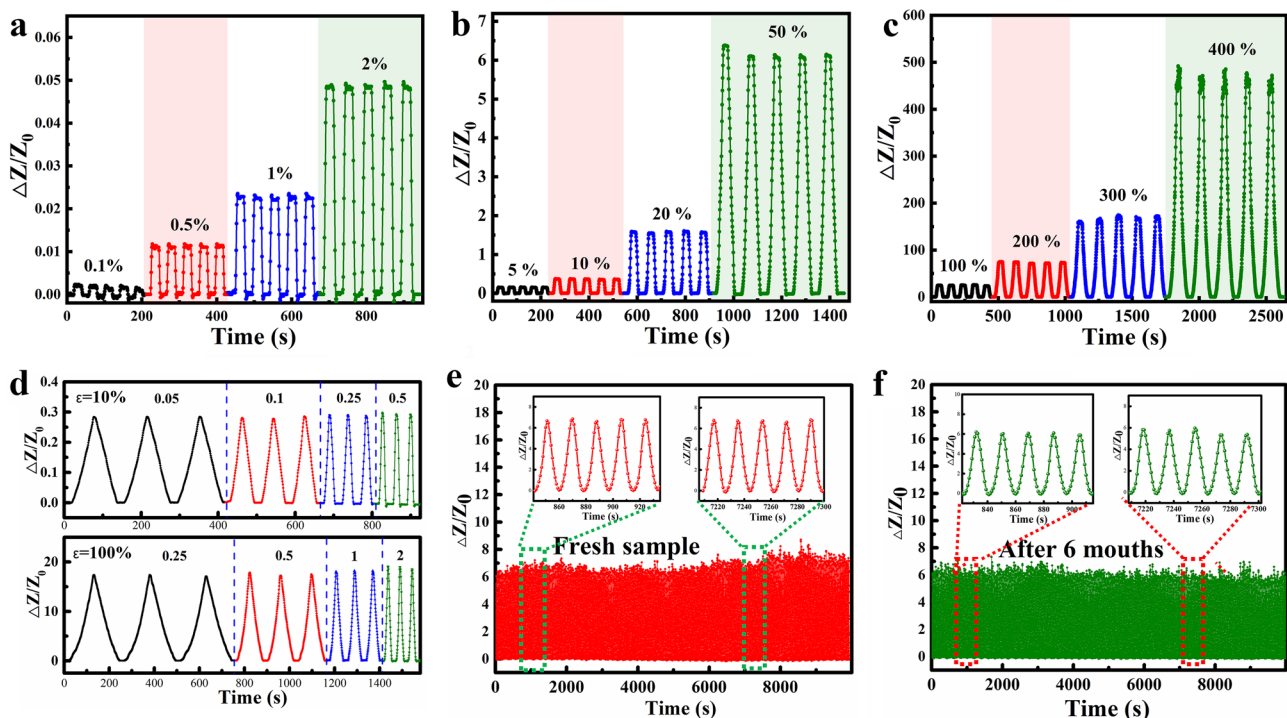


Fig. 4 Cyclic impedance response of CHPs-0.05-based strain sensor under **a, b, c** different strain amplitudes and **d** different strain rates. Cyclic impedance sensing stability of **e** CHPs-0.05-based strain sensor and **f** after being stored for 6 months at room temperature

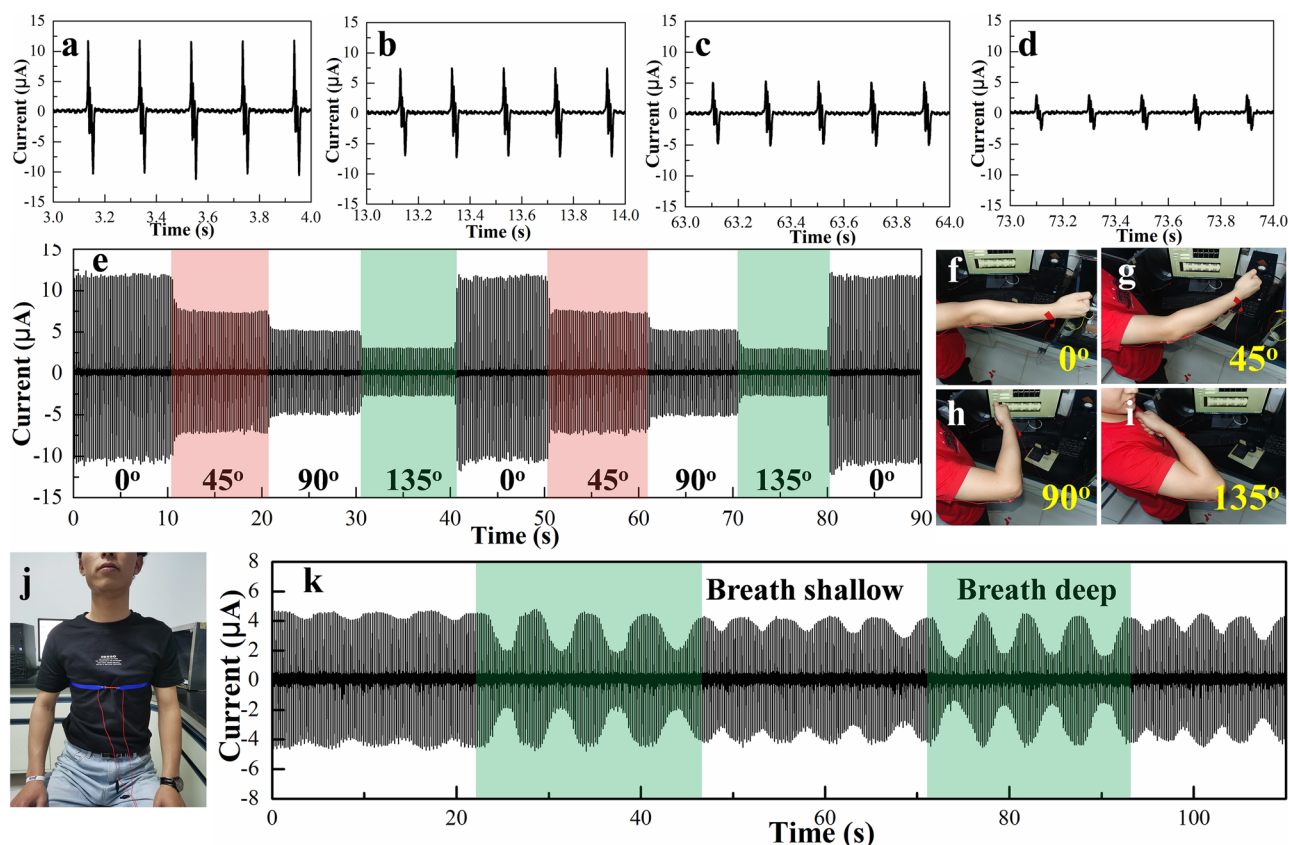


Fig. 5 Response behavior of CHPs-based strain sensor powered by friction power generation device to detect the human movements. **a–d** Current response of elbow joint bending at 0°, 45°, 90°, and 135°. **e**

Current response of elbow in continuous motion under different bending states. **f–i** Digital photos of elbow joint bending at 0°, 45°, 90°, and 135°. **j** Digital images and **k** current response of human breath

4 Conclusion

In summary, high-performance axon-like CHPs-based strain sensor was fabricated using CHPs as the core sensing medium, rubber tube as the elastic cortex substrate, and stainless steel as the electrode. The effect of ionic concentration on the impedance sensing behavior of the sensor was first investigated, the obtained impedance variation–strain curves of the sensor with different ionic concentrations displayed good symmetry in one stretching–releasing cycle, and a higher ionic concentration can lead to a lower sensitivity. To explain the impedance sensing mechanism of the sensor, an equivalent circuit model was built, and the variation of ion transport impedance and electric double-layer capacitance at the electrode–CHPs interface during the tension process were verified to be the internal sensing mechanism. Besides, the dynamic impedance response behavior of our prepared CHPs-based strain sensor also exhibited excellent stability and good consistency with the strain under different strain amplitudes and rates, which is unlike the baseline drift of the DC resistance sensing behavior of

the reported ionic hydrogel strain sensor. What is more, the special skin–core structure of the strain sensor can effectively solve the dehydration problem and poor mechanical property of hydrogel, and the amounts of interfaces between adjacent CHPs are also beneficial for improving the impedance responsivity. Finally, the CHPs-based strain sensor powered by the advanced wearable power generator of TENG also displays great potential application for real-time human motion and health monitoring.

Supplementary information The online version contains supplementary material available at <https://doi.org/10.1007/s42114-022-00437-y>.

Funding The research was financially supported by the National Natural Science Foundation of China (NO: 51803191, 12072325), the National Key R&D Program of China (2019YFA0706802), the 111 project (D18023), Key Scientific and Technological Project of Henan Province (202102210038).

Declarations

Conflict of interest The authors declare no competing interests.

References

- Li S, Xiao X, Hu J, Dong M, Zhang Y, Xu R, Wang X, Islam J (2020) Recent advances of carbon-based flexible strain sensors in physiological signal monitoring. *ACS Appl Electron Mater* 2(8):2282–2300. <https://doi.org/10.1021/acsaelm.0c00292>
- Wang D, Qin L, Yang W, He Y, Zhang S, Yang Y, Xu K, Gao P, Yu J, Cai K (2021) A conductive hydrogel based on galn and PVA/PAA/Fe³⁺ for strain sensor and physiological signal detection. *ACS Appl Polym Mater* 3(10):5268–5276. <https://doi.org/10.1021/acspap.1c01063>
- Pang Y, Yang Z, Han X, Jian J, Li Y, Wang X, Qiao Y, Yang Y, Ren T (2018) Multifunctional mechanical sensors for versatile physiological signal detection. *ACS Appl Mater & Inter* 10(50):44173–44182. <https://doi.org/10.1021/acsaami.8b16237>
- Bu Y, Shen T, Yang W, Yang S, Zhao Y, Liu H, Zheng Y, Liu C, Shen C (2021) Ultrasensitive strain sensor based on superhydrophobic microcracked conductive Ti₃C₂T_x MXene/paper for human-motion monitoring and E-skin. *Sci Bull* 66(18):1849–1857. <https://doi.org/10.1016/j.scib.2021.04.041>
- Liu H, Chen X, Zheng Y, Zhang D, Zhao Y, Wang C, Pan C, Liu C, Shen C (2021) Lightweight, superelastic, and hydrophobic polyimide nanofiber/MXene composite aerogel for wearable piezoresistive sensor and Oil/Water separation applications. *Adv Funct Mater* 31(13). <https://doi.org/10.1002/adfm.202008006>
- Chen J, Wang F, Zhu G, Wang C, Cui X, Xi M, Chang X, Zhu Y (2021) Breathable strain/temperature sensor based on fibrous networks of ionogels capable of monitoring human motion, respiration, and proximity. *ACS Appl Mater & Inter* 13(43):51567–51577. <https://doi.org/10.1021/acsaami.1c16733>
- Zhang J, Liu E, Hao S, Yang X, Li T, Lou C, Run M, Song H (2022) 3D Printable, ultra-stretchable, self-healable, and self-adhesive dual cross-linked nanocomposite ionogels as ultra-durable strain sensors for motion detection and wearable human-machine interface. *Chem Eng J* 431. <https://doi.org/10.1016/j.cej.2021.133949>
- Hang C, Zhao X, Xi S, Shang Y, Yuan K, Yang F, Wang Q, Wang J, Zhang D, Lu H (2020) Highly stretchable and self-healing strain sensors for motion detection in wireless human-machine interface. *Nano Energy* 76. <https://doi.org/10.1016/j.nanoen.2020.105064>
- Dong W, Yang L, Fortino G (2020) Stretchable human machine interface based on smart glove embedded with PDMS-CB strain sensors. *Ieee Sens J* 20(14):8073–8081. <https://doi.org/10.1109/jsen.2020.2982070>
- Chen J, Zhu Y, Chang X, Pan D, Song G, Guo Z, Naik N (2021) Recent progress in essential functions of soft electronic skin. *Adv Funct Mater* 31:2104686. <https://doi.org/10.1002/adfm.202104686>
- Chang X, Chen L, Chen J, Zhu Y, Guo Z (2021) Advances in transparent and stretchable strain sensors. *Adv Compos Hybrid Mater* 4(3):435–450. <https://doi.org/10.1007/s42114-021-00292-3>
- Zhang D, Xu S, Zhao X, Qian W, Bowen C, Yang Y (2020) Wireless monitoring of small strains in intelligent robots via a joule heating effect in stretchable graphene-polymer nanocomposites. *Adv Funct Mater* 30(13). <https://doi.org/10.1002/adfm.201910809>
- Guo Q, Zhang X, Zhao F, Song Q, Su G, Tan Y, Tao Q, Zhou T, Yu Y, Zhou Z, Lu C (2020) Protein-inspired self-healable Ti₃C₂ MXenes/rubber-based supramolecular elastomer for intelligent sensing. *ACS Nano* 14(3):2788–2797. <https://doi.org/10.1021/acsnano.9b09802>
- Tang L, Wu S, Qu J, Gong L, Tang J (2020) A review of conductive hydrogel used in flexible strain sensor. *Materials* 13(18). <https://doi.org/10.3390/ma13183947>
- Zhang D, Ren B, Zhang Y, Xu L, Huang Q, He Y, Li X, Wu J, Yang J, Chen Q, Chang Y, Zheng J (2020) From design to applications of stimuli-responsive hydrogel strain sensors. *J Mater Chem B* 8(16):3171–3191. <https://doi.org/10.1039/c9tb02692d>
- Sun X, Yao F, Li J (2020) Nanocomposite hydrogel-based strain and pressure sensors: a review. *J Mater Chem A* 8(36):18605–18623. <https://doi.org/10.1039/d0ta06965e>
- You I, Mackanic D, Matsuhisa N, Kang J, Kwon J, Beker L, Mun J, Suh W, Kim T, Tok J, Bao Z, Jeong U (2020) Artificial multimodal receptors based on ion relaxation dynamics. *Science* 370(6519):961–965. <https://doi.org/10.1126/science.aba5132>
- Jiang N, Hu D, Xu Y, Chen J, Chang X, Zhu Y, Li Y, Guo Z (2021) Ionic liquid enabled flexible transparent polydimethylsiloxane sensors for both strain and temperature sensing. *Adv Compos Hybrid Mater* 4(3):574–583. <https://doi.org/10.1007/s42114-021-00262-9>
- Zhou H, Lai J, Jin X, Liu H, Li X, Chen W, Ma A, Zhou X (2021) Intrinsically adhesive, highly sensitive and temperature tolerant flexible sensors based on double network organohydrogels. *Chem Eng J* 413:127544. <https://doi.org/10.1016/j.cej.2020.127544>
- Jiang N, Chang X, Hu D, Chen L, Wang Y, Chen J, Zhu Y (2021) Flexible, transparent, and antibacterial ionogels toward highly sensitive strain and temperature sensors. *Chem Eng J* 424:130418. <https://doi.org/10.1016/j.cej.2021.130418>
- Huang J, Peng S, Gu J, Chen G, Gao J, Zhang J, Hou L, Yang X, Jiang X, Guan L (2020) Self-powered integrated system of a strain sensor and flexible all-solid-state supercapacitor by using a high performance ionic organohydrogel. *Mater Horiz* 7(8):2085–2096. <https://doi.org/10.1039/d0mh00100g>
- Yang Y, Yang Y, Cao Y, Wang X, Chen Y, Liu H, Gao Y, Wang J, Liu C, Wang W, Yu J, Wu D (2021) Anti-freezing, resilient and tough hydrogels for sensitive and large-range strain and pressure sensors. *Chem Eng J* 403. <https://doi.org/10.1016/j.cej.2020.126431>
- Xu J, Wang G, Wu Y, Ren X, Gao G (2019) Ultrastretchable wearable strain and pressure sensors based on adhesive, tough, and self-healing hydrogels for human motion monitoring. *ACS Appl Mater & Inter* 11(28):25613–25623. <https://doi.org/10.1021/acsaami.9b08369>
- Li Z, He X, Cheng J, Li H, Zhang Y, Shi X, Yu K, Yang H, Ge Q (2021) Hydrogel-elastomer-based stretchable strain sensor fabricated by a simple projection lithography method. *Int J Smart Nano Mater* 12(3):256–268. <https://doi.org/10.1080/19475411.2021.1952335>
- Chen G, Huang J, Gu J, Peng S, Xiang X, Chen K, Yang X, Guan L, Jiang X, Hou L (2020) Highly tough supramolecular double network hydrogel electrolytes for an artificial flexible and low-temperature tolerant sensor. *J Mater Chem A* 8(14):6776–6784. <https://doi.org/10.1039/d0ta00002g>
- Sun X, Qin Z, Ye L, Zhang H, Yu Q, Wu X, Li J, Yao F (2020) Carbon nanotubes reinforced hydrogel as flexible strain sensor with high stretchability and mechanically toughness. *Chem Eng J* 382. <https://doi.org/10.1016/j.cej.2019.122832>
- Feng Y, Liu H, Zhu W, Guan L, Yang X, Zvyagin A, Zhao Y, Shen C, Yang B, Lin Q (2021) Muscle-inspired MXene conductive hydrogels with anisotropy and low-temperature tolerance for wearable flexible sensors and arrays. *Adv Funct Mater* 31(46):2105264. <https://doi.org/10.1002/adfm.202105264>
- Chen W, Liu L, Zhang H, Yu Z (2021) Kirigami-inspired highly stretchable, conductive, and hierarchical Ti₃C₂T_x MXene films for efficient electromagnetic interference shielding and pressure sensing. *ACS Nano* 15(4):7668–7681. <https://doi.org/10.1021/acsnano.1c01277>
- Chen L, Wang Z, Zhan Z, Xie M, Duan G, Cheng P, Chen Y, Duan H (2021) 3D printed super-anti-freezing self-adhesive human-machine interface. *Mater Today Phys* 19:100404. <https://doi.org/10.1016/j.mtphys.2021.100404>
- Shao L, Li Y, Ma Z, Bai Y, Wang J, Zeng P, Gong P, Shi F, Ji Z, Qiao Y, Xu R, Xu J, Zhang G, Wang C, Ma J (2020) Highly sensitive strain sensor based on a stretchable and conductive poly(vinyl alcohol)/phytic acid/NH₂-POSS hydrogel with a 3D microporous structure. *ACS Appl Mater & Inter* 12(23):26496–26508. <https://doi.org/10.1021/acsaami.0c07717>

31. Xu H, Shen Z, Gu G (2020) Performance characterization of ionic-hydrogel based strain sensors. *Sci China Technol Sci* 63(6):923–930. <https://doi.org/10.1007/s11431-019-1511-4>
32. Manandhar P, Calvert P, Buck J (2012) Elastomeric ionic hydrogel sensor for large strains. *Ieee Sens J* 12(6):2052–2061. <https://doi.org/10.1109/jsen.2011.2181993>
33. Kunzel M, Panhuis MI (2020) Strain sensors based on conducting poly(acrylamide) hydrogels. *MRS Adv* 5(17):917–925. <https://doi.org/10.1557/adv.2020.112>
34. Pan X, Wang Q, He P, Liu K, Ni Y, Chen L, Ouyang X, Huang L, Wang H, Xu S (2020) A bionic tactile plastic hydrogel-based electronic skin constructed by a nerve-like nanonetwork combining stretchable, compliant, and self-healing properties. *Chem Eng J* 379. <https://doi.org/10.1016/j.cej.2019.122271>

Publisher's Note Springer Nature remains neutral with regard to jurisdictional claims in published maps and institutional affiliations.